ADVANCED ENERGY MATERIALS
www.advenergymat.de

Probing the Diameter Limit of Single Walled Carbon Nanotubes in SWCNT: Fullerene Solar Cells

*Moritz Pfohl, Konstantin Glaser, Arko Graf, Adrian Mertens, Daniel D. Tune, Tanja Puerckhauer, Asiful Alam, Li Wei, Yuan Chen, Jana Zaumseil, Alexander Colsmann, Ralph Krupke, and Benjamin S. Flavel**

In this work, for the first time, the diameter limit of surfactant wrapped single walled carbon nanotubes (SWCNTs) in SWCNT:C_{60} solar cells is determined through preparation of monochiral small and large diameter nanotube devices as well as those from polychiral mixtures. Through assignment of the different nanotube chiralities by photoluminescence and optical density measurements a diameter limit yielding 0% internal quantum efficiency (IQE) is determined. This work provides insights into the required net driving energy for SWCNT exciton dissociation onto C_{60} and establishes a family of (*n*,*m*) species which can efficiently be utilized in polymer-free SWCNT:C_{60} solar cells. Using this approach the largest diameter nanotube with an IQE > 0% is found to be (8,6) with a diameter of 0.95 nm. Possible strategies to extend this diameter limit are then discussed.

1. Introduction

Single walled carbon nanotubes (SWCNTs) are becoming an established, photoactive material for use in organic solar cells. Besides their large intrinsic mobility (≈10^5 cm^2 V^{-1} s^{-1}),[1] this is primarily due to their structurally dependent optical and electronic properties. In the literature, the analogy of 'rolling up' a sheet of graphene to form a SWCNT is often used, where the "(*n*,*m*)" chiral index determines not only whether the SWCNT is metallic or semiconducting but also its diameter and the magnitude of the optical transitions.[2] It is this ability to select SWCNTs with desired optical gaps,[3] along with the commercial availability of nanotubes with a range of diameters, that make SWCNTs an interesting material that also offers potential avenues to tailor or extend the light absorption within established solar cells.[4] For example, in the case of a SWCNT with ≈1 nm diameter, light is absorbed in the infrared (S_{11} optical transition), visible (S_{22}), and UV (S_{33}) regimes. Through careful combination of the appropriate (*n*,*m*) species a close match to the solar spectrum is possible.[5] Indeed, in the simulation work of Tune and Shapter, an idealized tandem solar cell consisting of four small diameter nanotube species ((6,4), (9,1), (7,3), and (7,5) with diameters of 0.69–0.76 nm) that absorb mostly in the visible and the near infrared (up to 1024 nm) was predicted to have a sunlight harvesting potential of up to 28%.[6] Likewise, by instead choosing large diameter nanotubes (1.01–1.47 nm), which almost exclusively absorb in the near infrared and infrared (793–1682 nm), a sunlight harvesting potential of up to 19% was predicted in a semi-transparent organic solar cell. The respective model considered only the spectroscopic overlap between the nanotubes' absorption spectra and the terrestrial solar spectrum (AM1.5G) and implicitly assumed that all nanotubes can be used in a solar cell. Actually, the realization of a fully transparent solar cell from SWCNTs seems unlikely, especially with common fullerene-based acceptors (either C_{60} or [6,6]-phenyl $C_{61/71}$ butyric acid methyl ester ($PC_{61/71}BM$)) absorbing light between 300 and 800 nm along with other hole and electron blocking layers such as poly(3,4-ethylenedioxythiophene):polystyrene sulfonate (PEDOT:PSS) or bathocuproine and also minor contributions from S_{33}, especially for large diameter nanotubes, as discussed by Tune and Shapter.[6]

More fundamental to this discussion is that theoretical and experimental studies predict the requirement of a minimum energetic offset between the lowest unoccupied molecular

M. Pfohl, Dr. D. D. Tune, A. Alam, Prof. R. Krupke, Dr. B. S. Flavel
Institute of Nanotechnology
Karlsruhe Institute of Technology (KIT)
76021 Karlsruhe, Germany
E-mail: benjamin.flavel@kit.edu

M. Pfohl, A. Alam, Prof. R. Krupke
Institute of Materials Science
Technische Universität Darmstadt
64287 Darmstadt, Germany

K. Glaser, A. Mertens, T. Puerckhauer, Dr. A. Colsmann
Light Technology Institute
Karlsruhe Institute of Technology (KIT)
76131 Karlsruhe, Germany

A. Graf, Prof. J. Zaumseil
Institute for Physical Chemistry
Universität Heidelberg
69120 Heidelberg, Germany

Dr. D. D. Tune
Centre for Nanoscale Science and Technology
Flinders University
Adelaide 5042, Australia

Dr. L. Wei, Prof. Y. Chen
School of Chemical and Biomolecular Engineering
The University of Sydney
NSW 2006, Australia

DOI: 10.1002/aenm.201600890

orbital (LUMO) of the nanotube and that of the acceptor, that is necessary for exciton dissociation at the interface. The diameter dependent bandgap of SWCNTs therefore restricts the combination of (*n*,*m*) species or diameters that can be used for any specific acceptor molecule with fixed LUMO. In practice, the position of the LUMO in the SWCNT is calculated by adding the optical bandgap and exciton binding energy, which can be determined by the experimental findings of Dukovic et al.,[7] the analytic formula given by Capaz et al. and the scaling law proposed by Perebeinos et al.,[8,9] to the highest occupied molecular orbital (HOMO) of the nanotube.[10,11] In this way, the LUMO is approximated to the free carrier level. However, both the optical gap and the exciton binding energy are highly dependent on the surrounding dielectric environment. Therefore, in evaluating the actual diameter limit, it is important to distinguish between the two different SWCNT device architectures known from the literature, either a planar heterojunction or a bulk heterojunction (BHJ), but also between the two methods of preparation of the nanotubes. For BHJ solar cells, the SWCNTs are usually mixed with an acceptor with nanotube content below 10 wt% to reduce the probability of nanotube bundling and eventual trap states in the device. In this case, the surrounding dielectric environment can be assumed to be predominately defined by the acceptor molecule. Whereas, for planar solar cell designs, thin films of nanotubes are formed that can be either sparse, with 2%–3% light absorption, or dense, with more than 40% light absorption at the S_{11} transition for a 7 nm thick film.[12,13] In such a device layout the surrounding environment becomes a product of the film density, inter-tube interactions, and the adjacent layers on either side of the SWCNT film. The strength of these interactions is also dependent upon the method of nanotube preparation, be it through selective polymer wrapping or aqueous surfactant based routes. In the case of polymer wrapped SWCNT solar cells, despite efforts to remove the polymer after sorting, it is widely accepted that residual polymer remains on the sidewalls and therefore in the final device.[14] However, different strategies are now being developed to completely remove the polymer after sorting.[15] In the extreme case of high polymer content, this would afford a surrounding dielectric constant, ε, of approximately 3,[7] compared to 4.4 in the case of unwrapped nanotubes surrounded by C_{60} as an acceptor (SWCNT dielectric constant of ≥4).[9] This would in turn see the exciton binding energy in the nanotubes vary between 0.41 (ε = 3) and 0.24 eV (ε = 4.4) for (6,5) nanotubes with a diameter, d_t = 0.75 nm, or between 0.28 and 0.16 eV for (9,7) with d_t = 1.09 nm.[16]

For planar heterojunction solar cells of polymer wrapped (poly(9,9-dioctylfluorene) (PFO)) SWCNTs in conjunction with C_{60}, Bindl et al. pioneered the field and in 2010 they correlated the internal quantum efficiency (IQE) of five different nanotubes (7,5), (7,6), (8,6), (8,7), and (9,7) to the calculated exciton dissociation energy of the SWCNT:C_{60} interface.[10,17] Based on a reduction of IQE from 91% for the small diameter species of (7,5) to below 30% for the larger diameter (9,7), the authors concluded that above a nanotube diameter of 1 nm the excitons are no longer efficiently dissociated. However, the use of PFO in combination with the HiPco raw material that was used, provided the authors with only a narrow selection of (*n*,*m*) species. This prevented them from extending their measurement to larger diameters and identification of a cut-off point in the diameter range at which IQE is reduced to 0%. Wang et al. also investigated polymer wrapped SWCNTs (using regioregular poly(3-dodecylthiophene-2,5-diyl) (rr-P3DDT)) in planar solar cells but with the even smaller diameter CoMoCAT material (diameter distribution of 0.6–0.9 nm).[18] Although not specifically stated by the authors, it is apparent from comparing film absorption to external quantum efficiency measurements that nanotubes with an S_{11} optical transition greater than 1400 nm produce little, if any, photocurrent. For rr-P3DDT wrapped nanotubes in contact with C_{60} in a planar solar cell, the upper limit in terms of nanotubes with diameters still being able to dissociate excitons, should therefore be around 1.2 nm.

Bernardi et al. were the first to investigate the diameter cut-off in BHJ solar cells and suggested a diameter of 1.2 nm in combination with $PC_{61/71}BM$.[19] However, SWCNTs with a diameter of 1.2 nm would have S_{11} transitions up to 1500 nm (i.e., (12,5) with a diameter of 1.20 nm) and EQE data was only presented up to 1250 nm (diameter of ≈1 nm), which hinders the interpretation of the results. Likewise, Isborn et al. prepared BHJ solar cells consisting of SWCNT:C_{60} mixtures wrapped in graphene oxide and in contact with $PC_{61}BM$.[20] The authors tested the three different chiralities of (9,7), (7,6), and (6,5) and showed a decreasing short circuit current density (J_{SC}) for increasing diameters, which they interpreted to be a result of the decreasing efficiency of exciton dissociation. The findings were complemented by density functional theory (DFT) calculations. Despite solar cells consisting of (9,7) nanotubes outputting lower current and voltage, no EQE/IQE data was provided to clarify the question of whether (9,7) works less efficiently than (7,6) or (6,5), or even if (9,7) works at all (since it is possible to measure some photovoltaic output from similar SWCNT:C_{60} solar cells even in the absence of the SWCNTs. See discussion of exciting S_{22} of large diameter nanotubes at the end of this study). Most recently, Shastry et al. fabricated BHJ solar cells employing a mixture of $PC_{71}BM$, poly(3-hexylthiophene) (P3HT) and SWCNTs and demonstrated an increase in J_{SC} due to the broader absorption of polychiral nanotubes compared to monochiral devices, and showed a clear EQE signal from (8,7)-enriched SWCNTs at 1350 nm, which would correspond to a diameter of 1.02 nm.[21]

In recent work by Guillot et al. and by ourselves, transfer matrix calculations (TMCs) were used to evaluate the electric field intensity, $|E|^2$, within the solar cell stack, and changes in the acceptor layer thickness were shown to strongly modulate the EQE of devices due to resultant variation of $|E|^2$ at the plane of the nanotube film.[12,22] Following from these works, the conclusion can be drawn that for any investigation into a diameter cut-off not only is it important to consider the surrounding dielectric environment of the nanotubes, but also to ensure that the measurement reflects a true reduction in exciton dissociation and not an effect of decreasing electric field intensity at the wavelength of interest. In this work, we prepare planar SWCNT:C_{60} solar cells from polymer-free, monochiral SWCNTs of small ((6,5) and (7,5)) and large (9,8) diameter, along with polychiral mixtures of increasing diameter from the HiPco and arc discharge processes, with the aim of determining the diameter cut-off in polymer-free planar solar cell devices. In all cases, the nanotubes were prepared with surfactant-based methods. In

the case of using aqueous preparation processes, it is possible to have water filled and un-filled carbon nanotubes,[23] which due to the high dielectric constant of water (ε = 80)[24] might be expected to drastically increase the overall dielectric constant of the nanotube and in turn decrease the exciton binding energies. However, as calculated by Cambre et al.,[25] the presence of endohedral water only changes the effective dielectric constant up to 20% compared to the unfilled case. Regardless of whether the nanotubes are water filled or not, the use of sequential surfactant-based sorting has the advantage of maintaining the same dielectric environment across all devices and does not rely on different polymer systems to achieve the same richness in diameter range.

2. Results and Discussion

Throughout this work, a solar cell architecture consisting of a thin layer of SWCNTs (2–3 nm) in contact with C_{60} (115–127 nm) with a layer of PEDOT:PSS (41 ± 5 nm) as a hole transport layer and ITO front and silver back contacts were used. The device architecture is illustrated in **Figure 1**a and is similar to our previous work with polymer-free (6,5) SWCNT films.[12] However, unlike our previous work, the composition of the SWCNT film was varied from monochiral to polychiral dispersions with diameter distributions ranging from 0.7 to 1.8 nm. The optical absorption spectra of the aqueous dispersions and thin films were initially used to determine the (*n*,*m*) species distribution within each SWCNT film and were then compared to the EQE data, allowing an evaluation of the IQE for each nanotube type. In this way, a range of different (*n*,*m*) species and diameters were tested to determine which of them produces an IQE of 0%. The dispersions used for SWCNT films are shown in **Figure 2** and are labeled D1–D7 in order of increasing diameter. D1–D5 were obtained from the HiPco raw material and cover the diameter range 0.7–1.1 nm. D1 and D2 were monochiral suspensions of (6,5) and (7,5) with diameters of 0.75 and 0.82 nm, respectively. D3 was a near-monochiral suspension of (7,6) with a diameter of 0.88 nm. D4 and D5 were polychiral mixtures of nanotubes with mean diameters of 0.934 ± 0.006 and 0.939 ± 0.005 nm. Above this diameter range, monochiral suspensions of (9,8), with a diameter of 1.15 nm and labeled as D6, and polychiral dispersions from the arc discharge process, with a diameter range of 1.2–1.8 nm and labeled as D7, were used.

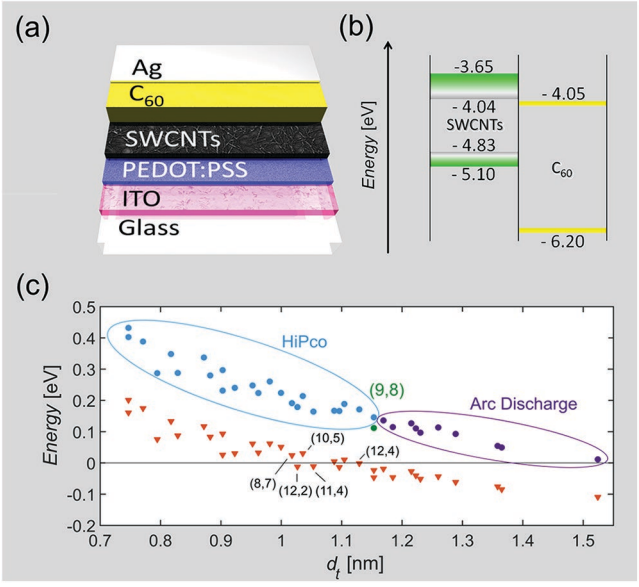

Figure 1. a) Schematic of the solar cell architecture. b) Energy diagram of SWCNTs with diameter between 0.7 and 1.8 nm and therefore variable bandgap, interfaced with C_{60}. Green bands indicate a sufficient energy offset between the LUMO HOMO (Q = –1) of the nanotubes and the LUMO (Q = 0) of C_{60}, according to the diagram shown in c), while white and grey indicate an insufficient energy offset. The net driving energy for exciton dissociation (triangles) is plotted in (c) along with the LUMO offset (dots) for SWCNTs with different diameters (d_t). Blue dots indicate nanotubes that are represented in dispersions from HiPco starting material while green and purple dots represent (9,8) enriched dispersions and dispersions from arc discharge starting material, respectively.

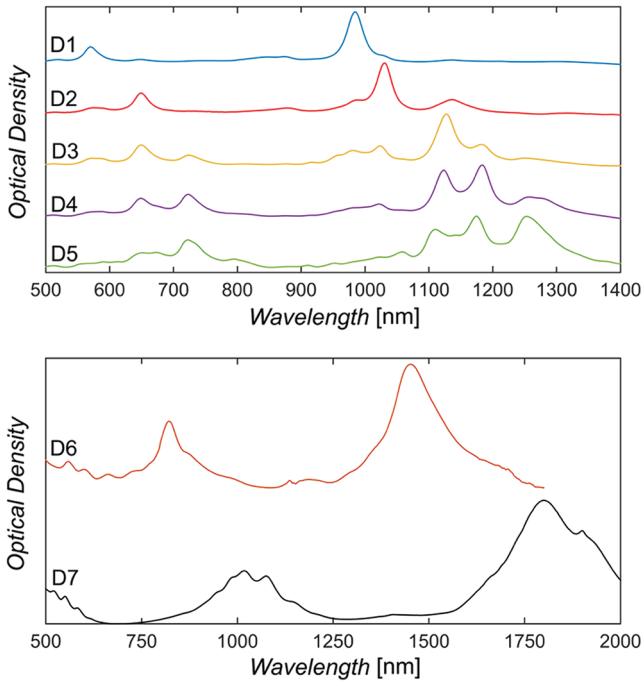

Figure 2. Optical density measurements on surfactant wrapped SWCNTs in dispersions made from HiPco (D1 to D5), (9,8) (D6) and arc discharge (D7) material.

Within the field of SWCNT:C_{60} solar cells it has become standard to discuss the HOMO/LUMO positions of the SWCNT, which, based on the LUMO offset to C_{60} and the exciton binding energy in the nanotubes, allows for a theoretical prediction to be made regarding the appropriate diameter range of SWCNTs for exciton dissociation at the C_{60} interface. In order to calculate the LUMO level of the SWCNTs, first photoelectron yield spectroscopy in air (PESA) was used to determine the HOMO energy of SWCNT films from all dispersions and a value of –4.83 eV for the arc discharge material through to –5.10 eV for (6,5) was measured. The PESA data can be found in Figure S1 in the Supporting Information. The HOMO energies of different nanotubes can also be calculated by assuming a Fermi level of –4.5 eV and adding half of the optical bandgap,

itself determined by adding 40 nm to the wavelength of the S_{11} transition in solution to account for the red-shift observed in experiments, which is in good agreement with the experimental findings.[12,26] According to the works of Spartau et al. and Bindl et al. the energy of the optical gap and the exciton binding energy (determined from the works of Dukovic et al. and Perebeinos et al.) are then added to the HOMO level to yield what is often referred to as the "LUMO" position of the SWCNT.[7,9–11] In effect this calculation affords the free carrier energy level of the nanotube and should more appropriately be referred to as HOMO ($Q = -1$). In all cases a dielectric constant of 4.4 for C_{60} was assumed and the exciton binding energy in the nanotubes was scaled in accordance with the work of Perebeinos et al.[9]

The LUMO of C_{60} was assumed to be constant at −4.05 eV as proposed by Shirley and Louie.[27] Using this information, a bandgap diagram for different (*n*,*m*) species can be drawn as shown in Figure 1b and the LUMO offset between SWCNTs and C_{60} can be used to determine the potential energy inherent in the system. By subtracting the exciton binding energy from the LUMO offset, the net driving energy can be calculated and if it is larger than zero, exciton dissociation is expected. This is plotted in Figure 1c. According to this calculation, solar cells made with nanotubes having diameters larger than the (8,7) or (10,5) (1.02 and 1.04 nm, respectively) should not be able to dissociate excitons at the interface with C_{60}, and should thus have IQE of 0%.

Central to this work is the accurate determination of the different SWCNT species in the film under investigation. This was achieved through a combination of optical absorption measurements of the aqueous dispersions used to make the films and photoluminescence (PL) measurements of the parent dispersions they were obtained from. Fitting was performed as fully described in the experimental details. Briefly Lorentzian profiles were used to fit S_{11} peaks and Gaussian profiles for fitting the exciton phonon sideband (EPS). The initial height and full width at half maximum (FWHM) was determined for optical density measurements and allowed to vary, broaden, respectively, for film absorbance measurements. The relative concentration of each (*n*,*m*) species found for optical density measurements of dispersions was varied within ±10% for the film absorbance measurement. The results of the fitting procedure are shown in **Figure 3** with results for monochiral (6,5) dispersion shown in Figure S2 in the Supporting Information.

SWCNT films from D1–D7 were then integrated into SWCNT:C_{60} solar cells and TMCs were employed to ensure sufficient electric field intensity $|E|^2$ at the position of the nanotubes with increasing diameter. In agreement with previous work,[12] the complex refractive indices for the SWCNT were ignored due to the thinness of the film and $|E|^2$ at the interface of PEDOT:PSS and C_{60} was considered. For all devices, a constant PEDOT:PSS thickness of 41 ± 5 nm was used and the C_{60} thicknesses varied from 115 to 127 nm for D2 to D5, 170 nm for D6 and 240 nm for D7. Film thicknesses were confirmed with a Dektak XT profiler and atomic force microscopy (AFM). Corresponding *J*–*V* curves are shown in Figure S3 in the Supporting Information and typical solar cell performance parameters are summarized in Table S1 in the Supporting Information, with fill factors ranging from 25% (D6) to 43% (D5). The mean absolute film absorbance is plotted in **Figure 4** along with EQE and the calculated $|E|^2$. The mean absorbance of each film shown in Figure 4 was calculated from measurements of the internal reflectance, which is shown in detail for D5 in Figure S4 in the Supporting Information and is discussed later in reference to IQE. In Figure 4 and Figure S5 in the Supporting Information, the shape of the EQE follows that of the optical absorbance of the monochiral (7,5) and (6,5) films (D2, D1, respectively) and is in agreement with previous work.[12] However, for D3 and D4, at around 1000 nm the shape of the EQE is dramatically different to that of the films' absorbance spectra (blue vs green curve).

For D5, an EQE peak around 1310 nm is visible but does not appear in the EQE spectra of D2–D4 (which represent devices made from material taken earlier in the sequential sorting process). Either the relative concentration of those SWCNTs was too small in D2–D4 or the nanotubes causing the EQE signal were not present in those previous dispersions. In the case of solar cells made from (9,8) and arc discharge material (D6 and D7), a notable absence of any nanotube contribution to the EQE is apparent in both Figure S6 in the Supporting Information and the raw current signals from all EQE measurements in this study, summarized in Figure S7 in the Supporting Information. It suggests that the diameter regime of 1.15–1.8 nm is above the cut-off point.

In order to quantify the contribution of each kind of nanotube to the solar cell performance, the measured EQE was fitted based on the predetermined (*n*,*m*) distribution in the film. In this case, the fitting procedure was kept rigid; the FWHM was not allowed to vary from the FWHM of the film and the peak position was constrained to be within −5 to +15 nm from the film to account for a changed dielectric environment (caused by nanotubes being sandwiched between air and glass compared to being sandwiched between PEDOT:PSS and C_{60}). The magnitude of each EQE peak was then allowed to vary freely between 0 and 100%. The results of the EQE fit are shown alongside the film absorbance spectra and calculated $|E|^2$ in Figure 4. It is apparent that the contribution to the EQE from small diameter SWCNTs such as (6,5) and (8,3) (0.75–0.77 nm) is stronger than expected from their concentration in the film, which is already a first indication of more efficient exciton dissociation for these SWCNTs. Although there are some contributions from (8,4) and (8,6) nanotubes detectable in optical density and PL measurements for D2, they do not show up in the fit of the EQE result. As the EQE contribution of each peak is allowed to vary freely, overlapping tube contributions, especially if some chiralities are only represented in minor quantities, can lead to neglecting tubes that should have a contribution to the overall EQE. Therefore we investigated solar cells with varying mixtures of different chiralities to draw a reliable conclusion on which nanotube is the last working one in the increasing diameter series of polymer-free SWCNT:C_{60} solar cells. By directly comparing the contribution of (9,5) and (8,7) to the EQE in Figure 4, we conclude that their contribution is either negligible or nonexistent. The same can also be observed for (9,7) and (10,6) in D4 and D5.

In order to eventually determine the cut-off of nanotube diameter/chirality beyond which exciton dissociation is not possible, in situ reflectance measurements were performed to

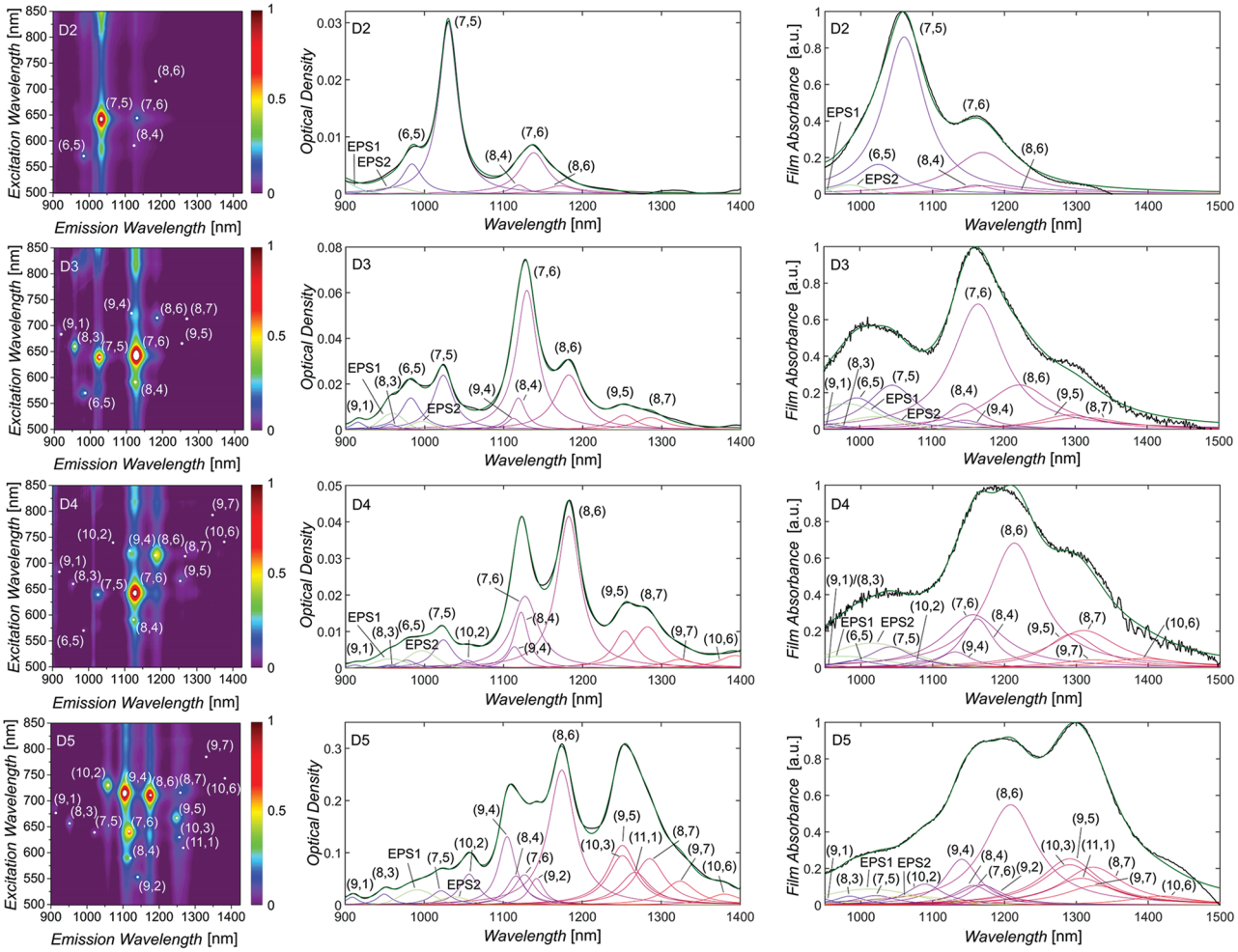

Figure 3. Photoluminescence contour map, corresponding optical density (measured with a 2 mm path length) and film absorbance measurements of SWCNT dispersions and films prepared from HiPco material. The sum of the Lorentzian S_{11} fits and the Gaussian shaped EPS is plotted in green, while the original optical density and film absorbance measurements are shown in black.

determine the absolute absorbance of the different nanotube films. From this, the IQE of all nanotubes under investigation was calculated. A scatter plot of the IQE of individual SWCNTs along with an exponential fit of the form $A \cdot e^{(b \cdot dt)}$ is shown in **Figure 5**. Compared to previous reported values on polymer-free, monochiral (6,5) SWCNT:C_{60} solar cells,[12] the IQE of the (6,5) nanotubes in the polychiral solar cell has decreased from 86% to 43%. This was partly attributed to the generation of trap states when interfacing large bandgap nanotubes and small bandgap nanotubes, and partly to intertube energy transfer amongst S_{11} transitions as outlined by Mehlenbacher et al.[28] Exciton dissociation at the SWCNT:C_{60} interface occurs on roughly the same time scale as the redistribution of energy to other S_{11} states (120 fs compared to ≈60 fs),[28,29] an increase in the number of alternative energy pathways likely causes a reduction in the total amount of excitons being dissociated at small diameter tubes and, consequently, the IQE of those junctions. Additionally, considering the comparable time scales, it becomes very difficult to distinguish between the generation of charge carriers from excitons being generated at the large diameter nanotubes and those that were generated from excitons being created on large band gap nanotubes and transferred onto small bandgap SWCNTs. Nevertheless, the recent study from Ihly et al. demonstrated an optimum LUMO offset between donor (SWCNTs) and acceptor (C_{60}) of ≈130 meV which is satisfied for small diameter (large bandgap) nanotubes, like (8,3), (9,1) or (6,5).[30] For larger or smaller LUMO offsets the relative carrier yield at the interface of donor and acceptor is clearly reduced and therefore the IQE of large diameter nanotubes. From these results we suggest an absolute upper bound diameter limit of 0.95 nm, corresponding to the (8,6) species. Beyond this diameter the required exciton dissociation energy is larger than that provided by the LUMO offset.

Upon comparing this finding to the cut-off values reported in the literature for polymer-wrapped nanotubes, the question arises why a significantly smaller diameter cut-off was obtained for polymer-free nanotubes (0.95 nm compared to up to 1.2 nm for polymer-wrapped nanotubes). Returning to the discussion about the net driving energy required for exciton dissociation at the SWCNT:C_{60} interface, the following set of equations can be used:

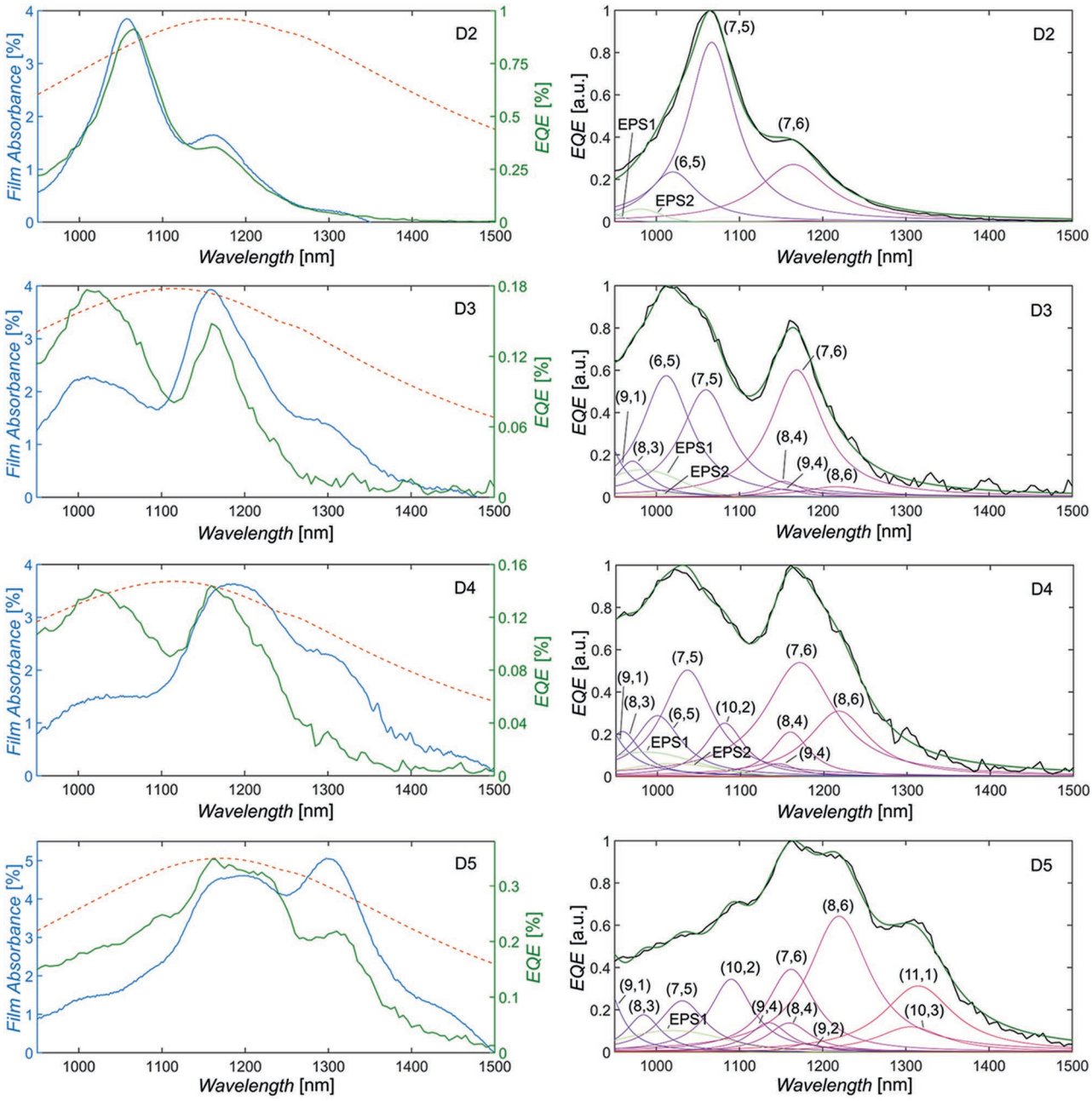

Figure 4. Mean film absorbance (blue), EQE (green) and $|E|^2$ (red) for solar cells prepared from HiPco material D2–D5 are shown in the left column. $|E|^2$ was scaled to the maximum film absorbance to guide the eye and to verify sufficient light intensity at the absorption of the nanotube film. In the right column the fit of the EQE is shown in green and the original measurement is shown in black.

$$\mathrm{LUMO}_{\mathrm{SWCNT}} - \mathrm{LUMO}_{\mathrm{C_{60}}} - E_{\mathrm{bind}} \geq 0 \quad (1)$$

$$\mathrm{HOMO}_{\mathrm{SWCNT}} + E_{\mathrm{S_{11}}} + E_{\mathrm{bind}} - \mathrm{LUMO}_{\mathrm{C_{60}}} - E_{\mathrm{bind}} \geq 0 \quad (2)$$

$$\mathrm{HOMO}_{\mathrm{SWCNT}} + E_{\mathrm{S_{11}}} - \mathrm{LUMO}_{\mathrm{C_{60}}} \geq 0 \quad (3)$$

According to Equation (3) it seems, that in determining the net driving energy, the binding energy of excitons E_{bind} in the SWCNTs cancels out. Thus, it may at first appear that changes in the dielectric environment of the nanotubes caused by the presence of the polymer wrapping and its effect on the exciton binding energy can be ruled out as an explanation for the observed difference in cut-off. However, the E_{S11} optical gaps of the nanotubes are themselves dependent on the dielectric environment since the optical gap is dependent on the electron–electron repulsion or self-energy and the binding energy, and both vary with the dielectric environment.[9,31] The net effect is that as the dielectric constant of the environment decreases, the optical gap increases. This can be readily seen when comparing the red-shifts of the optical gaps observed in solar cells versus those measured in solution. In the case of devices prepared

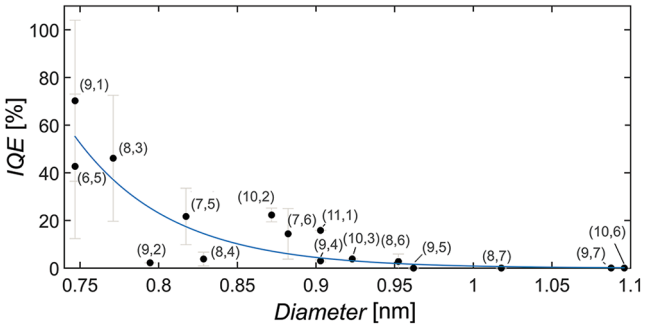

Figure 5. IQE values for nanotubes with different diameters (black dots). The best fit was obtained by an exponential function of the form $A \cdot \exp(b \cdot d_t)$ with $A = 11.26 \cdot 10^4$ and $b = -16.37$.

from polymer wrapped SWCNTs the red shift is around 6 meV (for a 7 nm thick film of (7,5) nanotubes reported by Bindl et al.,[32] that is even reduced upon increasing nanotube film thickness)[33] compared to around 42 meV for the same nanotubes, without the polymer, as used in this study and others.[34] A smaller red shift equates to a larger optical gap and therefore a larger net driving energy, as per Equation (3). Additionally, as shown in the work by Crochet et al., in the case of aggregated bundles of polymer-free SWCNTs the observed red-shift is not entirely captured by changes in the dielectric environment (increased screened Coulomb interaction between electron and holes) but also by a tunnelling induced splitting of the degenerate intertube conduction and valence bands that ultimately leads to delocalized excitons.[35] In summary, when going from polymer wrapped to polymer-free SWCNTs the optical gap decreases, which means that the net driving energy possessed by the junction decreases and therefore the maximum diameter (minimum gap) nanotube that will have a positive driving force for exciton separation at the junction decreases (required gap increases). A complicating factor in this analysis is that the binding energy, and thus LUMO energy, of the C_{60} is similarly dependent on the dielectric environment and is presumably thus also affected by the presence or absence of the polymer at the junction. Furthermore, the LUMO value for C_{60} used in Figure 1b does not take the free carrier state into account and is effectively a LUMO $Q = 0$ state. Therefore, the unrealistic comparison of a HOMO $Q = -1$ state in the SWCNT to a LUMO $Q = 0$ state in C_{60} is being made. Based on Shirley et al. the HOMO $Q = -1$ state in C_{60} can be calculated (based on the literature accepted HOMO value of –6.2 eV) to be –3.2 eV, which, in reference to Figure 1b, would result in none of the (n,m) species within the HiPco material contributing to the photocurrent.[12,17,27,34] As this is clearly not the case, the LUMO level used in this work must closely match reality and the HOMO level of the C_{60} must be different to the value often used in the SWCNT:C_{60} community. Using the HOMO/LUMO gap reported by Shirley et al., the HOMO level of C_{60} can be calculated to lie at around –7.05 eV.[27] However, the HOMO/LUMO gap of C_{60} has also been reported to vary between 2.6–3 eV and highlights the importance of measuring these values in situ in a SWCNT:C_{60} solar cell in the future.[36]

Considering the 0.95 nm diameter cut-off observed in this work (equivalent to a maximum wavelength of 1315 nm in the EQE), the ability to truly take advantage of the IR absorption properties of SWCNTs appears limited and the question arises as to what can be done to gain access to these larger diameters. One way to circumvent this limitation is to wrap the larger diameter nanotubes with a polymer such as the aforementioned rr-P3DDT, allowing the cut-off to be shifted to ≈1.2 nm (equivalent to a wavelength of 1500 nm). An alternative strategy was presented by Bernardi et al. for BHJ solar cells.[19] By introducing reduced graphene oxide (rGO), a highly disordered amorphous semiconductor with quasi metallic properties, in-between $PC_{61/71}BM$ and large diameter (>1.2 nm) SWCNTs, contributions to the photocurrent from nanotubes in the wavelength range from 1300 nm up to 1530 nm were demonstrated in the EQE data. With a dielectric constant for rGO of ≈30,[37] this clearly cannot be understood in terms of the dielectric environment model already described (which would predict the maximum accessible wavelength to decrease). However, they explained their finding in reference to the formation of large Schottky barriers for electrons between PCBM and rGO and therefore an energetically favoured hole transport from PCBM to rGO and finally onto SWCNTs. Perhaps the most obvious strategy is to change the acceptor to a material with a lower (more negative) LUMO energy than C_{60}. Often, fullerene derivatives like $PC_{61}BM$ or $PC_{71}BM$, with higher LUMO energies (at –3.96,[38] –3.95 eV,[39] respectively) are used as C_{60} alternatives. However, comparing the net driving energy of these acceptors to C_{60}, shown in **Figure 6**, would actually further decrease the number of available SWCNTs. Lowering the LUMO energy would cause a decrease in energy offset between the HOMO of the SWCNTs and the LUMO of acceptor, which is believed to reduce the V_{OC},[40] but by accessing the lower energy portion of the solar spectrum the available photon current could be significantly increased.[41] Clearly, if solar cells that operate further into the IR regime are desired, then new acceptor molecules with lower LUMO energies should be investigated. One alternative to C_{60} would be C_{70} (–4.09 eV).[42] This decrease in LUMO energy already shifts the net driving up so that larger diameter nanotubes up to (10,8) with a diameter of 1.23 nm are accessible. In order to successfully dissociate excitons from the full set of HiPco, (9,8) and arc discharge prepared SWCNTs, the LUMO level needs to be lowered even further. Two possibilities are C_{84} and $PC_{85}BM$,[39,42] (–4.44 and –4.31 eV, respectively, as outlined

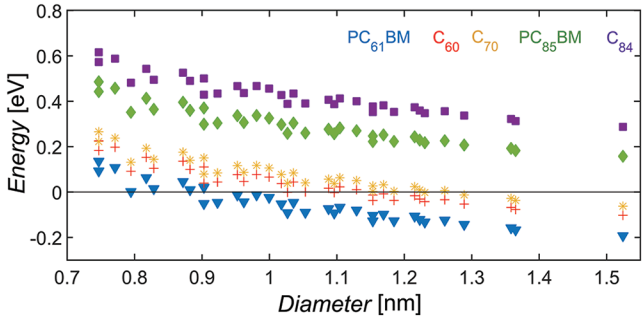

Figure 6. Net driving energy for different acceptor materials in contact with SWCNTs. The more negative the LUMO (highest value for $PC_{61}BM$ and smallest for C_{84}) the further the cut-off diameter shifts toward larger diameter/smaller bandgap nanotubes.

in the Supporting Information) which could, in theory, allow access to those nanotubes with diameters ≫ 1.5 nm as shown in Figure 6. Experimental evidence supporting this concept has previously been shown in solution experiments by Hilmer et al. through quenching of the nanotube PL by $PC_{85}BM$.[43] However, Ihly et al. demonstrated that increasing the LUMO offset (lowering the LUMO level of the acceptor) beyond the optimum of 130 meV, results in a decreasing carrier generation at the interface of SWCNTs and acceptor molecules.[30] In order to efficiently generate charge carriers in a SWCNT solar cell, different acceptors have therefore to be employed for different nanotube bandgap and diameter ranges. It seems as if the only way to exploit the full diameter range of HiPco and arc discharge SWCNTs in a solar cell is a tandem architecture with different acceptor molecules that ensure a LUMO offset being in the range of 130 meV.

An additional question that arises, particularly in the case of large diameter SWCNTs which do not possess a large enough bandgap to contribute to photocurrent generation via their fundamental S_{11} transition, is the possibility of photocurrent generation through the second optical transition (S_{22}). In the case of small diameter polymer-free and polymer wrapped SWCNTs, photocurrent has previously been shown to be generated from S_{22}.[5,12,22] In the case of large diameter SWCNTs such as those in D6 and D7, the bandgap of S_{22} should be large enough to provide a sufficient LUMO energy offset to C_{60}. We investigated this by first changing the C_{60} thickness to 124 nm to ensure high electric field intensity at the position of the S_{22} of D6 and D7, then measuring the EQE spectra. As shown in Figure S8c,f in the Supporting Information no photocurrent was observed from SWCNTs in the wavelength regime above 800 nm, corresponding to S_{22} of (9,8). According to the work of Lüer et al. and Mehlenbacher et al.,[44,45] excitons relax from S_{22} to S_{11} within ≈40 fs. Using two dimensional white light spectroscopy (2D-WL), Mehlenbacher et al. furthermore verified that energy is redistributed among S_{22} states on comparable time scales, and is about as fast as energy transfer among S_{11} states.[28,45] For the latter case, they stated that in mixed SWCNT chirality films, energy transfer from the smallest tube to the largest nanotube is equally likely as the transfer amongst nanotubes with almost equal diameters.[45] Dowgiallo et al. investigated the time scales of exciton dissociation and charge transfer from the S_{11} state of purified (6,5) SWCNTs onto C_{60}.[29] According to their findings, electrons are transferred from nanotubes to C_{60} within less than 120 fs. Comparing the different timescales, it is likely that the energy relaxation from S_{22} to S_{11} is happening faster than the exciton dissociation between S_{22} and C_{60} and that the S_{11} position of the nanotube determines whether there is an energy transfer from S_{22} to C_{60}. This idea is further supported by the higher binding energy for S_{22}, calculated by Ando,[46] despite a 2.4 times higher free carrier quantum yield for S_{22} excitons compared to S_{11} was shown by Park et al.[47]

3. Conclusions

To conclude, solar cells comprising SWCNT films with varying contents of small and large diameters were prepared and used in SWCNT:C_{60} solar cells. By careful assignment of the different component chiralities to PL measurements and subsequent fits to the optical spectra of dispersions, the distribution of nanotubes in each dispersion used in this study was derived. Employing these unique chirality distributions for subsequent fits to the optical spectra of SWCNT films made from these dispersions, and for EQE measurements of the corresponding solar cells, a direct assignment of each nanotube seen in EQE was possible. As a result, the largest polymer-free SWCNT to generate photocurrent in planar SWCNT:C_{60} solar cells has been determined to be the (8,6) nanotube with a diameter of 0.95 nm. The difference in diameter cut-off between the polymer-free nanotubes used in this study and the polymer wrapped nanotubes used in previous studies can be explained by a larger red-shift of the S_{11} optical transition in the polymer-free nanotubes, which can in turn be understood by considering the differences in dielectric environment in both cases. Additionally, the possibility of obtaining photocurrent by instead exciting the S_{22} transition of nanotubes with a diameter larger than the cut-off was ruled out in this study. As well as defining an upper limit of nanotube diameters that could be used in high efficiency SWCNT:C_{60} solar cells absorbing in the UV through to NIR, these results hold relevance in regards to the possibility of building solar cells from polymer-free SWCNTs that are (semi) transparent in the visible regime (400–800 nm) with the outcome being that to access the correct nanotube chiralities for that application, they must be interfaced with a different acceptor than C_{60}.

4. Experimental Section

Preparation of SWCNT Dispersions: SWCNT dispersions were prepared from aqueous surfactant wrapped dispersions using sodium dodecylsulfate (SDS, Merck), sodium cholate (SC ≥ 99%, Sigma Aldrich) and co-surfactant mixtures thereof. Detailed experimental details can be found in previous publications.[12,48] In brief small diameter HiPco (NanoIntegris) were suspended in 2 wt% SDS by sonication for 1 h followed by ultracentrifugation for 1 h at 64206·g (SW-40-TI rotor). The SDS concentration was then adjusted to 1.6 wt% SDS and added to 40 mL of Sephacryl-S200 gel (Amersham Biosciences). At 1.6 wt% SDS predominately (6,5) remained adsorbed to the gel and could be eluted with 1 wt% SC to afford dispersion D1. Following the separation of (6,5) the SDS concentration was gradually lowered in 0.2 wt% steps down to a concentration of 0.8 wt% and the process repeated to afford dispersions D2 to D5. In the case of large diameter nanotube dispersions, arc discharge material was obtained commercially (P2, Carbon Solutions) and (9,8) was selectively grown utilizing a sulfate-promoted catalyst approach in a chemical vapor deposition (CVD) process.[49] Semiconducting fractions of large diameter species were then prepared following the recent description for double walled carbon nanotubes (DWCNTs) by suspension in 1 wt% SC and the subsequent addition to a sephacryl column under 1 wt% SDS.[50] Dispersion absorption measurements were performed on a Varian Cary 500 spectrophotometer. For the (photoluminescence excitation) PLE maps of the SWCNT dispersion the spectrally separated output of a WhiteLase SC400 supercontinuum laser source (Fianium Ltd.) was used for excitation and spectra were recorded with an Acton SpectraPro SP2358 (grating 150 lines mm^{-1}) spectrometer with an OMA-V InGaAs line camera (Princeton Instruments) and corrected for background and wavelength-dependent sensitivity/excitation power.

Preparation of SWCNT Films: SWCNT films were prepared via the method of EDSA.[12] Briefly, silicon oxide (SiO_2) wafers were covered with poly(methyl methacrylate) (PMMA 950K 0.25 µm $(4000\ rpm)^{-1}$,

Allresist), baked (160 °C, 30 min) and immersed vertically in the SWCNT dispersion in an oven (60 °C, 6 h). Copious washing with deionized water was used to remove any residual surfactant on the nanotubes. The SWCNT film was then scored into a rectangle (≈1.3 cm^2 in size) and slowly immersed into water to detach the SWCNT coated PMMA from the SiO_2. Prior to the final detachment of the film, the substrate was withdrawn from the water, re-immersed in glycerol (99.5%, VWR), and transferred onto glass for characterization. Scanning electron microscopy (SEM) (Zeiss Ultra Plus), AFM (Bruker Dimension Icon) using silicon cantilevers (Mikromasch, 325 kHz, 40 Nm^{-1}), and film absorbance measurements (Varian Cary 500 spectrophotometer) were taken to characterize the nanotube films. The HOMO level of all films were measured on a glass substrate at 800 nW by PESA (AC-2E, Riken Keiki).[51]

Detailed Fitting Procedure: Assignment of the (*n*,*m*) species in a PL contour map was performed using a modified approach from Bachilo et al. by individually fitting the parameters a1 to a3 and b1 to b3 for mod($n - m$) = 1 and mod($n - m$) = 2 SWCNTs for each dispersion to calculate the first (ν_{11}) and second (ν_{22}) van Hove transition frequencies, as proposed by Cambré et al.[52,53] Fitting was performed with an unconstrained, non-linear least square solver, "lsqnonlin," using MATLAB R2014b:

$$\nu_{11} = \frac{1\times10^7\ \mathrm{cm}^{-1}}{a_1 + a_2 \times d_t} + \frac{a_3 \times \cos(3\alpha)}{d_t^2} \tag{4}$$

$$\nu_{22} = \frac{1\times10^7\ \mathrm{cm}^{-1}}{b_1 + b_2 \times d_t} + \frac{b_3 \times \cos(3\alpha)}{d_t^2} \tag{5}$$

The transition frequencies in Equations (4) and (5) depend on the diameter (d_t) and the chiral angle (α) of the individual SWCNT. Each diameter and chiral angle was calculated based on the formulas given by Pipes et al., assuming a C–C bond length of 0.142 nm.[54] The results of these assignments are shown in Figure 3. Using the assignment from photoluminescence contour maps, the S_{11} regions of the dispersion absorption measurements were fitted with Lorentzian functions after subtracting a background as described by Nair et al.[55] Fitting was again performed with a constrained, non-linear least square solver, "lsqnonlin," using MATLAB R2014b. The quality of the fit of a nonlinear equation strongly depends on the starting values of the fit. Therefore, the initial FWHM of each (*n*,*m*) species was calculated based on the position of S_{11} in the units of eV ($E^{(n,m)}{}_{11}$) as proposed empirically by Tune and Shapter:[6]

$$\mathrm{FWHM}_{(n,m)} = 0.067 \times E_{11}^{(n,m)} - 0.02 \tag{6}$$

This initial FWHM was divided by a factor of two to match the measurements and was converted into wavelength and allowed to increase or decrease during fitting within ± 20% for SWCNTs with an S_{11} smaller or equal to 1050 nm. For nanotubes with S_{11} transitions larger than 1050 nm, an increase in FWHM of 20% was not sufficient for an accurate fit. The upper limit of Lorentzian broadening was therefore allowed to increase up to 60% of the initial FWHM. The initial peak position was based on the set of S_{11} positions for HiPco SWCNTs provided by Bachilo et al.[52] Employing the built in MATLAB function "findpeaks," local maxima of the optical density plots were detected. The position of these peaks was then compared to the data set of initial S_{11} positions for HiPco SWCNTs and assigned to specific (*n*,*m*) chiralities. All peak positions that could be assigned this way were allowed to vary within ±5 nm during the fitting. Remaining nanotubes, that could not be detected automatically, were allowed to vary between −5 and +20 nm of their recorded S_{11} position. Also the height of the peaks was allowed to vary during fitting. The lower limit was set to be 10% of the initial peak height, while the upper limit was set case sensitive: for dispersions with only a few chiralities, one peak usually represented one tube. For mixed chiralities a peak can represent a convolution of many different (*n*,*m*) species with unknown spectral weight and therefore unknown height. Based on this observation, the upper bound of the peak height was set to 95% of the initial peak height for dispersions with only a few nanotubes and to 90% for dispersions with mixed chiralities. Additionally, a Gaussian curve for the exciton phonon side band (EPS) was introduced with a starting FWHM of 40 nm, which was allowed to vary between 50% and 200% (20–80 nm). The spectral weight transfer of S_{11} to the phonon side band was also modeled based on the diameter dependence suggested by Perebeinos et al in Equation (7):[56]

$$\frac{I_{EPS}}{I_{S_{11}}} = 0.017 + \frac{0.1\ \mathrm{nm}}{d_t} + f_1 \tag{7}$$

whereas I_{EPS} is the spectral weight of the exciton phonon side band and I_{S11} is the spectral weight of the first optical transition. The correction factor f_1 was introduced in this study to account for a modified weight transfer due to changes in dielectric environment or an increase in bundling and was allowed to vary during fitting between ±0.07. The necessity of the correction factor f_1 is verified in Figure S9 in the Supporting Information. The position of the EPS was set to be 0.200 eV above the S_{11} transition and allowed to vary within ±0.005 eV. The results of this fitting procedure are shown in Figure 3. Additionally the relative concentration of each (*n*,*m*) species was determined by dividing the area of a specific tube by the sum of all areas and is tabulated along with the center and FWHM of each nanotube in Table S2 to Table S4 in the Supporting Information.

As described in the previous work,[12] evaporation driven self-assembly (EDSA) was used to prepare the thin SWCNTs films from dispersions D1–D7. Representative SEM images of SWCNT films can be found in Figure S10 in the Supporting Information, where sparse films with optical densities of 2%–5% are depicted. In the next step, film absorbance measurements were fitted based on the (*n*,*m*) distribution determined from dispersion. Prior to fitting the film, the background was subtracted following the procedure outlined by Tian et al.[57] The sum of a Fano and Lorentzian profile was used to account for inter-band electronic transition at the M saddle point of the Brillouin zone (≈4.5 eV) and the π Plasmon resonance (≈5.3 eV), respectively. An example of the background subtraction procedure for both the dispersion and thin film measurements is provided in Figure S11 in the Supporting Information. In accordance with previous reports a broadening and red-shift of all peaks was observed and was accounted for by applying a constant factor between 1 and 2.5 to the FWHM of all Lorentzian and 1 to 3 for all Gaussians.[58]

The red-shift itself was modeled to vary between 0 and +40 nm with an initial guess of +30 nm. The relative concentration of each nanotube was also allowed to vary between ±10% compared to the relative concentration calculated for dispersion measurements. This deviation was necessary to compensate uncertainties introduced by film formation and subsequent background subtraction. For the EPS, Equation (7) was used to calculate f_1 and was allowed to vary between −0.05 and 0.1. These higher upper boundary conditions were set to reflect the larger part of the spectral weight to be transferred from S_{11} onto the EPS in a film of mixed chiralities. For the measurements of D1 and D2, nearly monochiral (6,5), (7,5), a smaller part of the spectral weight as proposed by Perebeinos et al. was transferred in the film fitting, as confirmed by the fitting results listed in Table S5 in the Supporting Information. For mixed chiralities a smaller part (negative f_1) was transferred for solution fits, but a larger one for film measurements.

Solar Cell Preparation: PEDOT:PSS (AI 4083, Ossila) was filtered (Millex-HV, 0.45 µm, Merck) and mixed with ethanol (absolute, VWR) in ratios of 1:1 before sonication for 10 min. This mixture was then spin coated (40 µL at 2200 rpm for 60 s, yielding a thickness of 41 ± 5 nm) and baked in inert atmosphere (250 °C, 10 min) before being covered with PMMA (40 nm). SWCNT films floating on glycerol were subsequently transferred onto the sample and left in chloroform (≥99.8%, Sigma-Aldrich) over night. Following electric field intensity calculations, different thicknesses of C_{60} (99.9+%, Sigma Aldrich) were evaporated at 380–450 °C through a shadow mask in a Lesker SPECTROS Evaporation System (base pressure: 7–9 × 10^{-7} Pa) with the layer thickness monitored by quartz crystals. A 100 nm silver top

electrode was evaporated to complete the fabrication of solar cells with areas of 0.105 cm^2. Internal reflectance measurements were carried out on a Bruker microscope (Vertex 80/Hyperion 2000 FTIR). Film thicknesses were measured with a DektakXT profiler (Bruker) and an AFM (Bruker Dimension Icon) using silicon cantilevers (Mikromasch, 325 kHz, 40 Nm^{-1}).

Solar Cell Characterization: The solar cells were characterized with a Keithley 238 source meter under AM1.5G illumination from a Newport 300 W solar simulator (M-91160). The solar simulator was calibrated using a silicon reference cell (91150-KG5, Newport). Following *J–V* characterization, the EQE was measured with a 450 W Xenon light source, an optical chopper (473.5 Hz), a 300 mm monochromator (LOT-Oriel), a custom designed current amplifier (DLPCA-S, Femto Messtechnik) and a digital lock-in amplifier (eLockin 203 Anfatec). Initial calibration was carried out with a calibrated UV-enhanced silicon (SM1PD2A, Thorlabs) and germanium diode (FDG03-CAL, Thorlabs).

Transfer Matrix Calculations: Transfer matrix calculations were performed using a modified MATLAB code available from the McGehee group at Stanford and as outlined by Burkhard et al. and Pettersson et al.[59] The complex refractive indices of glass, ITO, PEDOT:PSS and C_{60} were determined with a LOT Woolam Vaiable Angle Spectroscopic Ellipsometry (VASE) Ellipsometer and included in the code. The electric field intensity was calculated for all solar cells presented in this study.

Supporting Information

Supporting Information is available from the Wiley Online Library or from the author.

Acknowledgements

B.S.F. gratefully acknowledges support from the Deutsche Forschungsgemeinschaft (DFG) under grant numbers FL 834/1-1 and FL 834/2-1. R.K. acknowledges funding by the DFG under INST 163/354-1 FUGG. K.G., A.M., T.P., and A.C. acknowledge funding by the German Federal Ministry for Education and Research (BMBF) under contract 03EK3504 (project TAURUS) and support by the DFG Centre for Functional Nanostructures (CFN). A.G. and J.Z. acknowledge financial support by European Research Council under the European Union's Seventh Framework Programme (FP/2007-2013)/ERC Grant Agreement No. 306298. Y.C. acknowledges support from the Faculty of Engineering and Information Technologies, The University of Sydney, under the Faculty Research Cluster Program. R.K., B.S.F., Y.C., and W.L. acknowledge support from the Singaporean–German Researcher Mobility Scheme. The views expressed herein are those of the authors and are not necessarily those of the Faculty.

Received: April 28, 2016
Revised: July 6, 2016
Published online:

[1] T. Dürkop, S. A. Getty, E. Cobas, M. S. Fuhrer, *Nano Lett.* **2003**, *4*, 35.
[2] a) M. S. Dresselhaus, G. Dresselhaus, R. Saito, A. Jorio, *Phys. Rep.* **2005**, *409*, 47; b) H. Kataura, Y. Kumazawa, Y. Maniwa, I. Umezu, S. Suzuki, Y. Ohtsuka, Y. Achiba, *Synth. Metals* **1999**, *103*, 2555.
[3] M. Engel, K. E. Moore, A. Alam, S. Dehm, R. Krupke, B. S. Flavel, *ACS Nano* **2014**, *8*, 9324.
[4] D. D. Tune, F. Hennrich, S. Dehm, M. F. G. Klein, K. Glaser, A. Colsmann, J. G. Shapter, U. Lemmer, M. M. Kappes, R. Krupke, B. S. Flavel, *Adv. Energy Mater.* **2013**, *3*, 1091.
[5] D. J. Bindl, M. S. Arnold, *J. Phys. Chem. C* **2013**, *117*, 2390.
[6] D. D. Tune, J. G. Shapter, *Energy Environ. Sci.* **2013**, *6*, 2572.
[7] G. Dukovic, F. Wang, D. Song, M. Y. Sfeir, T. F. Heinz, L. E. Brus, *Nano Lett.* **2005**, *5*, 2314.
[8] R. B. Capaz, C. D. Spataru, S. Ismail-Beigi, S. G. Louie, *Phys. Rev. B* **2006**, *74*, 121401.
[9] V. Perebeinos, J. Tersoff, P. Avouris, *Phys. Rev. Lett.* **2004**, *92*, 257402.
[10] D. J. Bindl, M. Y. Wu, F. C. Prehn, M. S. Arnold, *Nano Lett.* **2011**, *11*, 455.
[11] C. D. Spataru, S. Ismail-Beigi, L. X. Benedict, S. G. Louie, *Phys. Rev. Lett.* **2004**, *92*, 077402.
[12] M. Pfohl, K. Glaser, J. Ludwig, D. D. Tune, S. Dehm, C. Kayser, A. Colsmann, R. Krupke, B. S. Flavel, unpublished.
[13] M. J. Shea, M. S. Arnold, *Appl. Phys. Lett.* **2013**, *102*, 243101.
[14] D. J. Bindl, M. J. Shea, M. S. Arnold, *Chem. Phys.* **2013**, *413*, 29.
[15] a) Y. Joo, G. J. Brady, M. J. Shea, M. B. Oviedo, C. Kanimozhi, S. K. Schmitt, B. M. Wong, M. S. Arnold, P. Gopalan, *ACS Nano* **2015**, *9*, 10203; b) I. Pochorovski, H. Wang, J. I. Feldblyum, X. Zhang, A. L. Antaris, Z. Bao, *J. Am. Chem. Soc.* **2015**, *137*, 4328; c) J. Han, Q. Ji, H. Li, G. Li, S. Qiu, H.-B. Li, Q. Zhang, H. Jin, Q. Li, J. Zhang, *Chem. Commun.* **2016**, *52*, 7683.
[16] A. F. Hebard, R. C. Haddon, R. M. Fleming, A. R. Kortan, *Appl. Phys. Lett.* **1991**, *59*, 2109.
[17] D. J. Bindl, N. S. Safron, M. S. Arnold, *ACS Nano* **2010**, *4*, 5657.
[18] H. Wang, G. I. Koleilat, P. Liu, G. Jiménez-Osés, Y.-C. Lai, M. Vosgueritchian, Y. Fang, S. Park, K. N. Houk, Z. Bao, *ACS Nano* **2014**, *8*, 2609.
[19] M. Bernardi, J. Lohrman, P. V. Kumar, A. Kirkeminde, N. Ferralis, J. C. Grossman, S. Ren, *ACS Nano* **2012**, *6*, 8896.
[20] C. M. Isborn, C. Tang, A. Martini, E. R. Johnson, A. Otero-de-la-Roza, V. C. Tung, *J. Phys. Chem. Lett.* **2013**, *4*, 2914.
[21] T. A. Shastry, S. C. Clark, A. J. E. Rowberg, K. A. Luck, K.-S. Chen, T. J. Marks, M. C. Hersam, unpublished.
[22] S. L. Guillot, K. S. Mistry, A. D. Avery, J. Richard, A.-M. Dowgiallo, P. F. Ndione, J. van de Lagemaat, M. O. Reese, J. L. Blackburn, *Nanoscale* **2015**, *7*, 6556.
[23] a) S. Cambré, B. Schoeters, S. Luyckx, E. Goovaerts, W. Wenseleers, *Phys. Rev. Lett.* **2010**, *104*, 207401; b) J. A. Fagan, J. Y. Huh, J. R. Simpson, J. L. Blackburn, J. M. Holt, B. A. Larsen, A. R. H. Walker, *ACS Nano* **2011**, *5*, 3943.
[24] C. G. Malmberg, A. A. Maryott, *J. Res. Natl. Bur. Stand.* **1956**, *56*, 1.
[25] S. Cambré, S. M. Santos, W. Wenseleers, A. R. T. Nugraha, R. Saito, L. Cognet, B. Lounis, *ACS Nano* **2012**, *6*, 2649.
[26] V. Barone, J. E. Peralta, J. Uddin, G. E. Scuseria, *J. Chem. Phys.* **2006**, *124*, 024709.
[27] E. L. Shirley, S. G. Louie, *Phys. Rev. Lett.* **1993**, *71*, 133.
[28] R. D. Mehlenbacher, J. Wang, N. M. Kearns, M. J. Shea, J. T. Flach, T. J. McDonough, M.-Y. Wu, M. S. Arnold, M. T. Zanni, *J. Phys. Chem. Lett.* **2016**, *7*, 2024.
[29] A.-M. Dowgiallo, K. S. Mistry, J. C. Johnson, J. L. Blackburn, *ACS Nano* **2014**, *8*, 8573.
[30] R. Ihly, K. S. Mistry, A. J. Ferguson, T. T. Clikeman, B. W. Larson, O. Reid, O. V. Boltalina, S. H. Strauss, G. Rumbles, J. L. Blackburn, *Nat. Chem.* **2016**, *8*, 603.
[31] J. Jiang, R. Saito, G. G. Samsonidze, A. Jorio, S. G. Chou, G. Dresselhaus, M. S. Dresselhaus, *Phys. Rev. B* **2007**, *75*, 035407.
[32] D. J. Bindl, A. J. Ferguson, M.-Y. Wu, N. Kopidakis, J. L. Blackburn, M. S. Arnold, *J. Phys. Chem. Lett.* **2013**, *4*, 3550.
[33] A. J. Ferguson, A.-M. Dowgiallo, D. J. Bindl, K. S. Mistry, O. G. Reid, N. Kopidakis, M. S. Arnold, J. L. Blackburn, *Phys. Rev. B* **2015**, *91*, 245311.
[34] R. M. Jain, R. Howden, K. Tvrdy, S. Shimizu, A. J. Hilmer, T. P. McNicholas, K. K. Gleason, M. S. Strano, *Adv. Mater.* **2012**, *24*, 4436.

[35] J. J. Crochet, J. D. Sau, J. G. Duque, S. K. Doorn, M. L. Cohen, *ACS Nano* **2011**, *5*, 2611.
[36] M. S. Dresselhaus, G. Dresselhaus, P. C. Eklund, in *Science of Fullerenes and Carbon Nanotubes*, Academic Press, San Diego, **1996**, 464.
[37] J. Y. Kim, T. Kim, J. W. Suk, H. Chou, J. H. Jang, J. H. Lee, I. N. Kholmanov, D. Akinwande, R. S. Ruoff, *Small* **2014**, *10*, 3405.
[38] B. W. Larson, J. B. Whitaker, X.-B. Wang, A. A. Popov, G. Rumbles, N. Kopidakis, S. H. Strauss, O. V. Boltalina, *J. Phys. Chem. C* **2013**, *117*, 14958.
[39] F. B. Kooistra, V. D. Mihailetchi, L. M. Popescu, D. Kronholm, P. W. M. Blom, J. C. Hummelen, *Chem. Mater.* **2006**, *18*, 3068.
[40] N. K. Elumalai, A. Uddin, *Energy Environ. Sci.* **2016**, *9*, 391.
[41] S. Rühle, *Solar Energy* **2016**, *130*, 139.
[42] Y. Yang, F. Arias, L. Echegoyen, L. P. F. Chibante, S. Flanagan, A. Robertson, L. J. Wilson, *J. Am. Chem. Soc.* **1995**, *117*, 7801.
[43] A. J. Hilmer, K. Tvrdy, J. Zhang, M. S. Strano, *J. Am. Chem. Soc.* **2013**, *135*, 11901.
[44] L. Lüer, J. Crochet, T. Hertel, G. Cerullo, G. Lanzani, *ACS Nano* **2010**, *4*, 4265.
[45] R. D. Mehlenbacher, T. J. McDonough, M. Grechko, M.-Y. Wu, M. S. Arnold, M. T. Zanni, *Nat. Commun.* **2015**, *6*, 6732.
[46] T. Ando, *J. Phys. Soc. Jpn.* **2004**, *73*, 3351.
[47] J. Park, O. G. Reid, J. L. Blackburn, G. Rumbles, *Nat. Commun.* **2015**, *6*, 8809.
[48] B. S. Flavel, K. E. Moore, M. Pfohl, M. M. Kappes, F. Hennrich, *ACS Nano* **2014**, *8*, 1817.
[49] a) H. Wang, B. Wang, X.-Y. Quek, L. Wei, J. Zhao, L.-J. Li, M. B. Chan-Park, Y. Yang, Y. Chen, *J. Am. Chem. Soc.* **2010**, *132*, 16747; b) H. Wang, L. Wei, F. Ren, Q. Wang, L. D. Pfefferle, G. L. Haller, Y. Chen, *ACS Nano* **2013**, *7*, 614.
[50] K. E. Moore, M. Pfohl, D. D. Tune, F. Hennrich, S. Dehm, V. S. K. Chakradhanula, C. Kübel, R. Krupke, B. S. Flavel, *ACS Nano* **2015**, *9*, 3849.
[51] M. Uda, *Jpn. J. Appl. Phys.* **1985**, *24*, 284.
[52] S. M. Bachilo, M. S. Strano, C. Kittrell, R. H. Hauge, R. E. Smalley, R. B. Weisman, *Science* **2002**, *298*, 2361.
[53] S. Cambré, W. Wenseleers, *Angew. Chem. Int. Ed.* **2011**, *50*, 2764.
[54] a) M. S. Dresselhaus, G. Dresselhaus, R. Saito, *Carbon* **1995**, *33*, 883; b) R. B. Pipes, S. Frankland, P. Hubert, E. Saether, *Comp. Sci. Technol.* **2003**, *63*, 1349.
[55] N. Nair, M. L. Usrey, W.-J. Kim, R. D. Braatz, M. S. Strano, *Anal. Chem.* **2006**, *78*, 7689.
[56] V. Perebeinos, J. Tersoff, P. Avouris, *Phys. Rev. Lett.* **2005**, *94*, 027402.
[57] Y. Tian, H. Jiang, I. V. Anoshkin, L. J. I. Kauppinen, K. Mustonen, A. G. Nasibulin, E. I. Kauppinen, *RSC Adv.* **2015**, *5*, 102974.
[58] a) M. J. O'Connell, S. M. Bachilo, C. B. Huffman, V. C. Moore, M. S. Strano, E. H. Haroz, K. L. Rialon, P. J. Boul, W. H. Noon, C. Kittrell, J. Ma, R. H. Hauge, R. B. Weisman, R. E. Smalley, *Science* **2002**, *297*, 593; b) S. Reich, C. Thomsen, P. Ordejón, *Phys. Rev. B* **2002**, *65*, 155411.
[59] a) G. F. Burkhard, E. T. Hoke, M. D. McGehee, *Adv. Mater.* **2010**, *22*, 3293; b) L. A. A. Pettersson, L. S. Roman, O. Inganäs, *J. Appl. Phys.* **1999**, *86*, 487.